ISBN: 978-3-95450-231-8 ISSN: 2673-5490 doi: 10.18429/JACoW-IPAC2023-TUPA064

EXPERIMENTAL STUDIES AND SIMULATIONS FOR AN X-BAND SHORT-PULSE ULTRA-HIGH GRADIENT PHOTOINJECTOR*

G. Chen†, D. Doran, S. Kim, W. Liu, J. Power, C. Whiteford, E. Wisniewski,
Argonne National Laboratory, Lemont, IL 60439, USA
C. Jing[1], E. Knight, S. Kuzikov, Euclid Techlabs LLC, Bollingbrook, IL 60440, USA
E. Frame, X. Lu[1], P. Piot[1], Northern Illinois University, DeKalb, IL 60115, USA
[1] also at Argonne National Laboratory, Lemont, IL 60439, USA

Abstract

A program is under way at the Argonne Wakefield Accelerator (AWA) facility, in collaboration with Euclid Techlabs and Northern Illinois University (NIU) to develop a GV/m-scale photocathode gun, with the goal of producing bright electron bunches. The novel X-band (11.7 GHz) photo-gun (Xgun) is powered by high-power, short rf pulses (9 ns), which are generated by the AWA drive beam in a wakefield structure. In the first series of experiments, the Xgun produced ~ 400 MV/m peak field on the photocathode surface [1]. The Xgun has also shown exceptional robustness, with no noticeable breakdown observed after being fully conditioned. As a first step towards achieving a complete understanding of the Xgun's performance, we aim to investigate the fundamentals of photoemission in the high-gradient regime. Systematic simulations will be presented for the near-future photocathode thermal emittance measurements.

INTRODUCTION

The development of high-brightness photoinjectors is a key technology for various scientific instruments such as future linear colliders, next-generation free-electron lasers (FELs) [2], compact X-ray sources [3], and ultrafast electron diffraction or microscopy (UED/UEM) [4, 5]. An increase in beam brightness can be accomplished by a reduction of the thermal emittance, and an increase of the accelerating field at the photocathode surface. The Argonne Wakefield Accelerator (AWA) facility, in collaboration with Euclid Techlabs and Northern Illinois University (NIU), is taking the latter approach by attempting to increase E_z in an rf gun to unprecedented levels. The collaboration is developing an ultra-high gradient X-band photogun (Xgun) that uses the short rf pulse (~9 ns) approach at room temperature, motivated by the fact that decreasing the rf pulse length reduces the probability of rf breakdown [6].

During the first set of experiments, the Xgun generated a peak field of ~400 MV/m on the surface of the cathode [1] with the rf conditioning history shown in Figure 1 (a), where the *Ratio* parameter is calculated from measured rf signals and simulated rf signals. Values *Ratio* < 1 indicates a discrepancy between the measured rf signal and the simulated (or expected) rf signal which may be caused by the rf breakdowns (or dark current–induced beam loading). In a more recent rf test as shown in Figure 1 (b), which took place almost two years after the initial conditioning test and involved frequent air exposure for beamline element installation, the Xgun demonstrated exceptional robustness, with no noticeable breakdown observed after full conditioning.

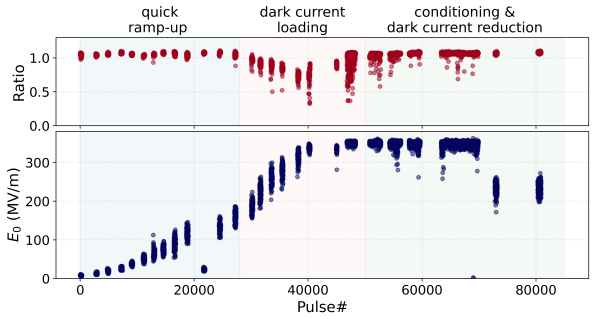

(a) initial high power rf conditioning test in 2020 [1]

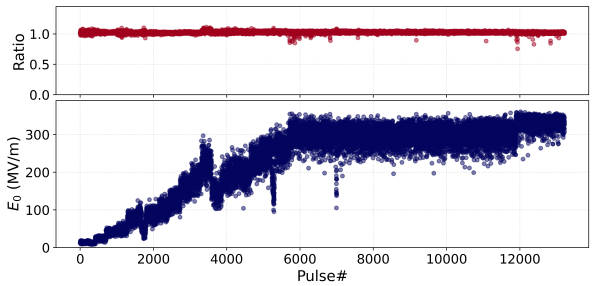

(b) Xgun robustness test in 2022

Figure 1: Comparison of two high-power rf tests of the Xgun performed nearly two-year apart.

While some beam parameters have been measured and reported in Ref. [1, 7], further studies are still needed to understand the performance of the photocathode at this high gradient regime such as the Schottky effects as observed in Ref [1] and possible onset of emittance degradation due to physical and chemical roughness [8]. As the first step towards fully characterizing the beam properties of the Xgun, we aim to investigate the fundamentals of photoemission in the high-gradient regime. In this work, systematic simulations (using `ASTRA`) have been conducted in order to provide

* This work is supported by the U.S. DOE, under award No. DE-SC0022010 to NIU, DOE SBIR grant No. DE-SC0018709 at Euclid Techlabs LLC, and contract No. DE-AC02-06CH11357 with ANL. At ANL, this work is partially supported by Laboratory Directed Research and Development (LDRD) funding.
† b288079@anl.gov

ISBN: 978-3-95450-231-8 ISSN: 2673-5490 doi: 10.18429/JACoW-IPAC2023-TUPA064

general guidance for upcoming cathode thermal emittance measurements.

EXPERIMENTAL SETUP

Laser system

A simplified schematic diagram of the laser system appears in Figure 2. An optical delay stage in the laser path is used to adjust the relative phase between the laser pulse and the Xgun field. A microlens-array (MLA) block is inserted to ensure the uniformity of the laser profile [9], an iris and a few focusing lenses are installed to achieve the desired laser spot size on the cathode surface.

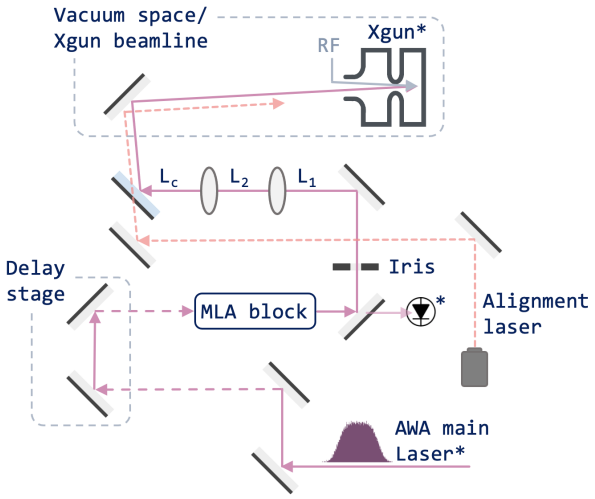

Figure 2: Schematic of the laser-transport system before injection in the Xgun.

Xgun beamline

In Figure 3, a schematic diagram of the current version of the Xgun beamline is presented. A few key elements of the beamline include a 1.5-cell Xgun (more details on its rf properties can be found in Ref. [1, 10]), a main solenoid with an iron plate installed to reduce the residue B_z on cathode surface, a beam position monitor (BPM) that can also be used for low charge measurement, an imaging solenoid for emittance measurements, and a spectrometer dipole for energy measurements.

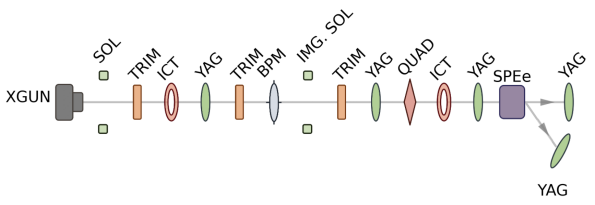

Figure 3: Diagram of the Xgun beamline.

SIMULATIONS FOR THERMAL EMITTANCE MEASUREMENTS

The projected emittance (expressed in Eqn. 1) can be calculated from the quadrature sum of the thermal emittance ($\varepsilon_{\text{therm}}$), which is the goal of the measurement, other contributions include rf emittance (ε_{rf}), as well as emittance growth terms from solenoid aberrations ($\varepsilon_{\text{optics}}$) and space charge effects (ε_{sc}). To obtain an accurate measurement of the thermal emittance, it is necessary to minimize any potential contribution to emittance growth from other sources.

$$\varepsilon_{\text{x}} = \sqrt{\varepsilon_{\text{therm}}^2 + \varepsilon_{\text{rf}}^2 + \varepsilon_{\text{optics}}^2 + \varepsilon_{\text{sc}}^2} \tag{1}$$

In this section, the simulated thermal emittance is simply estimated based on the excess energy of 0.1 eV in ASTRA. The reduced work function caused by Schottky effects at high gradients will be studied and expected to be compensated by a non-collinear optical parametric amplifier (NOPA) pumped at 392 nm.

Rf effects

Given the scaling of the rf emittance $\varepsilon_{\text{rf}} \propto E_0 \sigma_x^2 \sigma_z^2$ [11], where σ_x is the transverse beam size and σ_z is the bunch length, the rf phase variation in different beam slices can cause a growth in the projected emittance. At AWA, laser pulse length can be adjusted from 300 fs (FWHM) to 6 ps. To study the impact of rf effects and minimize ε_{rf} that is solely due to unsuitable bunch lengths, simulated emittance at the Xgun exit for the available laser-pulse durations is shown in Figure 4. In these simulations, transverse beam size (σ_x) on the cathode surface is set to 0.1 mm, E_0 is fixed to 350 MV/m, space charge force is neglected, both solenoids are turned off (i.e. no residue B_z on the cathode). Figure 4, indicates that the laser-pulse duration needs to be kept below 900 fs to avoid a noticeable impact on the emittance.

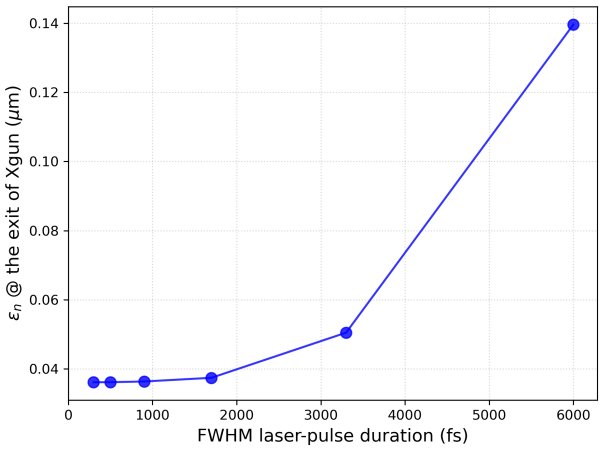

Figure 4: Simulation of normalized emittance at the exit of the Xgun as a function of laser-pulse durations that are available for use at AWA.

ISBN: 978-3-95450-231-8 ISSN: 2673-5490 doi: 10.18429/JACoW-IPAC2023-TUPA064

Solenoid modification and solenoid effects

When the Xgun is operated at a high gradient (350 MV/m), a non-zero residual B_z was found on the cathode surface with the main solenoid set to ~0.24 T, which has a noticeable contribution to the projected emittance. Therefore, an iron plate has been designed and installed to the solenoid; the simulated on-axis B_z is shown in Figure 5. This results in a reduction of the residual B_z on the cathode to < 22 Gauss. The effect of the iron plate on the resulting emittance is plotted in Figure 6.

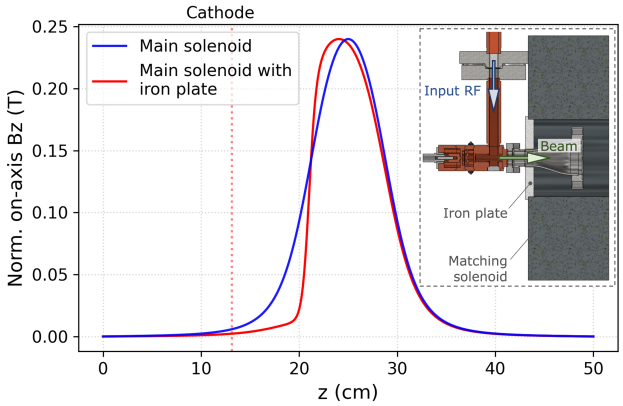

Figure 5: Comparison of on-axis B_z field of the main solenoid with and without the iron plate; the red dashed line indicates the position of the cathode. Inset: cross-sectional view of the Xgun and the main solenoid in the beamline.

Additionally, the solenoid effects (e.g. chromatic and spherical aberrations) may also lead to an increase of emittance (i.e. $\varepsilon_{\text{optics}}$). Given the relations of $\varepsilon_{\text{chromatic}} \propto K\sigma_p\sigma_x^2$ and $\varepsilon_{\text{spherical}} \propto \sigma_x^4$ [12], where K is the focal strength of the solenoid and σ_p is the momentum spread, σ_x is a dominate factor and needs to be carefully adjusted to avoid possible contributions from solenoid effects.

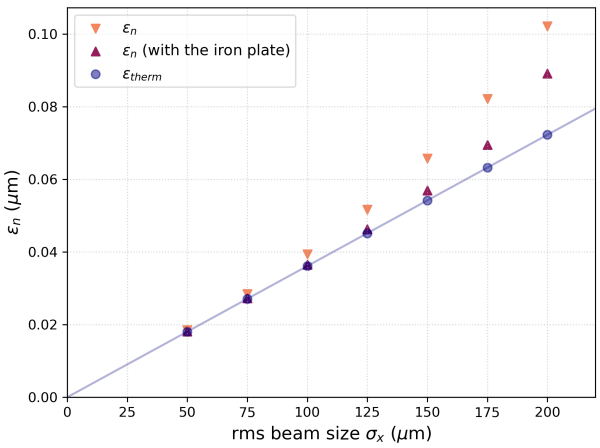

Figure 6: Simulated emittance at the end of the beamline as a function of the rms beam spot size. $\varepsilon_{\text{therm}}$ is thermal emittance estimated based on the excess energy of ~0.1 eV.

Figure 6 demonstrates the simulated emittance against different beam spot sizes with a bunch length of 300 fs and space charge force is neglected. To minimize the solenoid effects, the rms beam size needs to be maintained at ≤ 125 μm.

Space-charge effects

The space charge effect is another key factor that could cause the emittance to grow. Considering the constraints on the bunch length (≤ 900 fs) and the transverse beam size (≤ 125 μm), Figure 7 illustrates the simulated emittance evolution as the bunch charge increases, where the longest allowed bunch length of 900 fs was selected in order to mitigate the space charge effects.

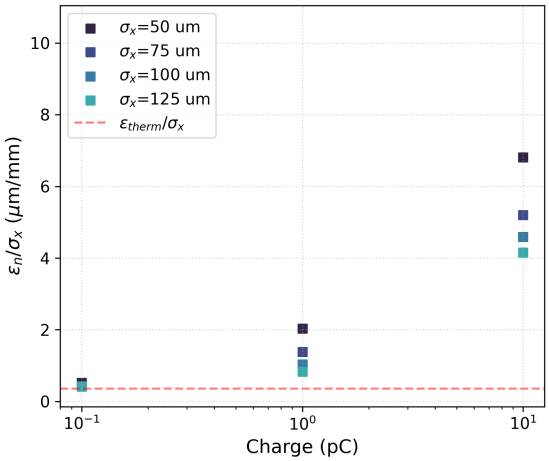

Figure 7: Simulated emittance per rms beam size as a function of bunch charge; the red dashed line is the thermal emittance per rms beam size. For each charge, four cases of laser spot size on the photocathode are simulated (see legend).

As shown in Figure 7, noticeable space-charge effects were observed at a charge level of ~1 pC. However, due to the uncertainties in the initial beam distribution, it is challenging to accurately simulate the electron beams with the presence of nonlinear space charge forces; these results can only provide a rough estimate of the electron charge level at which space charge effects may become significant. This emittance growth term ε_{sc} will be minimized during the experiment since one practical way to demonstrate the insignificance of space charge dynamics is that the measured emittance converges to a constant level below a certain charge threshold.

CONCLUSION

In this work, systematic simulations were performed in order to provide general guidance for the planned cathode thermal-emittance measurements.

ISBN: 978-3-95450-231-8 ISSN: 2673-5490 doi: 10.18429/JACoW-IPAC2023-TUPA064

REFERENCES

[1] W. H. Tan, S. Antipov, D. S. Doran, G. Ha, C. Jing, E. Knight, S. Kuzikov, W. Liu, X. Lu, P. Piot, J. G. Power, J. Shao, C. Whiteford, and E. E. Wisniewski, "Demonstration of sub-GV/m accelerating field in a photoemission electron gun powered by nanosecond X-band radio-frequency pulses", Phys. Rev. Accel. Beams 25, 083402 (2022).

[2] P. Emma, R. Akre, J. Arthur, R. Bionta, C. Bostedt, J. Bozek, A. Brachmann, P. Bucksbaum, R. Coffee, F.-J. Decker et al.,"First lasing and operation of an ångstrom-wavelength free-electron laser", Nat. Photonics 4, 641 (2010).

[3] W.S. Graves, J. Bessuille, P. Brown, S. Carbajo, V. Dolgashev, K.-H. Hong, E. Ihloff, B. Khaykovich, H. Lin, K. Murari, E.A. Nanni, G. Resta, S. Tantawi, L.E. Zapata, F.X. Kärtner, and D.E. Moncton, Phys. Rev. ST Accel. Beams 17, 120701 (2017) https://doi.org/10.1103/PhysRevSTAB.17.120701

[4] F. Qi, Z. Ma, L. Zhao, Y. Cheng, W. Jiang, C. Lu, T. Jiang, D. Qian, Z. Wang, W. Zhang, P. Zhu, X. Zou, W. Wan, D. Xiang, and J. Zhang, "Breaking 50 Femtosecond Resolution Barrier in MeV Ultrafast Electron Diffraction with a Double Bend Achromat Compressor", Phys. Rev. Lett. 124, 134803 (2020).

[5] R. Li and P. Musumeci, "Single-Shot MeV Transmission Electron Microscopy with Picosecond Temporal Resolution", Phys. Rev. Appl. 2, 024003 (2014).

[6] V. Dolgashev, S. Tantawi, Y. Higashi, and B. Spataro, "Geometric dependence of radio-frequency breakdown in normal conducting accelerating structures", Applied Physics Letters, vol. 97, no. 17, p. 171501, Oct. 2010. doi:10.1063/1.3505339

[7] G. Chen and *et al.*, "Emittance Measurements and Simulations from an X-Band Short-Pulse Ultra-High Gradient Photoinjector" doi:10.18429/JACoW-NAPAC2022-MOZE3

[8] G.S. Gevorkyan, S. Karkare, S. Emamian, I.V. Bazarov, and H.A. Padmore, "Effects of physical and chemical surface roughness on the brightness of electron beams from photocathodes", Phys. Rev. Accel. Beams 21, 093401 (2018).

[9] A. Halavanau, *et al.*, "Spatial control of photoemitted electron beams using a microlens-array transverse-shaping technique", Phys. Rev. Accel. 20, 103404 (2017). doi:10.1103/PhysRevAccelBeams.20.103404

[10] S. Kuzikov, S. Antipov, P. Avrakhov, E. Dosov, G. Ha, C. Jing, E. Knight, W. Liu, X. Lu and P. Piot, *et al.* "An X-Band Ultra-High Gradient Photoinjector", doi:10.18429/JACoW-IPAC2021-WEPAB163

[11] K-J. Kim, "Rf and space-charge effects in laser-driven rf electron guns", Nuclear Instruments and Methods in Physics Research A275 (1989) 201-218.

[12] David H. Dowell, 2016, "Sources of emittance in RF photocathode injectors: Intrinsic emittance, space charge forces due to non-uniformities, RF and solenoid effects", arXiv:1610.01242